AJNR

Reduced-Distortion Diffusion MRI of the Craniovertebral Junction

M. Iima, A. Yamamoto, V. Brion, T. Okada, M. Kanagaki, K. Togashi and D. Le Bihan

Reduced-Distortion Diffusion MRI of the Craniovertebral Junction

M. Iima
A. Yamamoto
V. Brion
T. Okada
M. Kanagaki
K. Togashi
D. Le Bihan
🔓

BACKGROUND AND PURPOSE: CVJ lesion suffers from a high sensitivity to susceptibility and distortion artifacts, which sometimes makes diffusion image difficult to interpret. Our purpose was to evaluate the potential for diffusion MR imaging using RS-EPI compared with SS-EPI in the assessment of the CVJ.

MATERIALS AND METHODS: RS-EPI and SS-EPI DTI images were acquired from 10 healthy volunteers using 3T MRI with a 32-channel head coil. For both sequences, the following parameters were used: 1-mm^2 in-plane resolution; 3-mm section thickness; TR = 5200 ms; 1 acquisition at $b = 0$ and 12 different encoding directions at $b = 1000$ seconds/mm^2. The RS-EPI sequence scan time was 9.44 minutes (1 average). The SS-EPI sequence was 9.37 minutes (8 averages). Diffusion tensor calculation and image analysis were performed using DTIStudio software. Diffusion trace images and color-coded fiber orientation maps were evaluated by 2 independent readers for distortion and delineation of fine structure using a semiquantitative scale in selected landmark locations. The absolute distances between the temporal base and the cerebellar contour between the T2-weighted images and the diffusion trace images obtained with RS-EPI and SS-EPI were also compared.

RESULTS: The contours of the temporal lobe and cerebellum were better delineated and distortion artifacts were clearly reduced with the RS-EPI sequence. More fine structures were also visible in the brain stem and cerebellum with the RS-EPI sequence. The amount of distortion was significantly reduced with RS-EPI compared with SS-EPI ($P < .01$).

CONCLUSIONS: The RS-EPI DTI sequence was less prone to geometric distortion than the SS-EPI sequence and allowed a better delineation of CVJ internal structure. Although the acquisition time is still relatively long, the RS-EPI appears as a promising approach to perform DTI studies in CVJ lesions, such as brain stem ischemia, neurodegenerative diseases, brain and skull base tumors, or inflammation.

ABBREVIATIONS: CVJ = craniovertebral junction; FA = fractional anisotropy; GRAPPA = generalized autocalibrating partially parallel acquisition; MD = mean diffusivity; RS = readout–segmented; SS = single-shot

DWI and DTI have become standards for evaluating neurologic disorders such as acute brain ischemia, intracranial lesions, and white matter diseases.[1,2] However, diffusion MR imaging has not been so successful in investigating lesions near the CVJ. The CVJ is a complex structure consisting of the occiput (posterior skull base), the atlas and axis vertebrae, and supporting ligaments. The proximity of the CVJ with the skull base and the sinuses results in significant magnetic susceptibility artifacts, to which EPI-based sequences are prone. Geometric distortion, signal intensity dropouts, or hyperintense signals are frequent, sometimes making diffusion images difficult to interpret.[3] However, there is clearly a clinical need to image the CVJ area with great detail for the diagnosis and management of CVJ lesions caused by ischemia, malformation, tumors, infection, or injury. Both ADC and other DTI

parameters, such as FA, MD,[4] or fiber tract delineation, should be obtained with some degree of confidence.

So far, DTI images have been acquired mainly using SS-EPI sequences, which are very robust to motion artifacts and allow very short acquisition times compatible with clinical needs. SS-EPI sequences are, however, very sensitive to susceptibility artifacts because of the spin dephasing that occurs during the relatively long echo trains necessary to collect data from the whole k-space within 1 echo signal intensity. This pitfall has been shown as an important limitation in the diagnosis of middle ear cholesteatoma.[5] An alternative is to split the acquisition of k-space points in segments, through the use of multiple shots to decrease the length of the signal intensity acquisition window.[6] Multiple shot–EPI is more robust to such susceptibility artifacts, especially when used with acceleration techniques such as GRAPPA.[7] Multishot techniques are, however, sensitive to motion that occurs between shots. Such pitfalls can be overcome with navigator echo techniques,[8-10] which can be combined with RS-EPI and improved through the reacquisition of corrupted data.[11] With this RS-EPI approach, reduced-distortion images with high resolution and reduced blurring from T2* signal intensity decay, compared with SS-EPI, have been obtained,[11] even at very high fields.[12] The superiority of this approach has been demonstrated for DWI in a clinical setting,[13] including in the pediatric

Table 1: Distortion using a semiquantitative scale

Scale (0–4)
4	Perfect contour continuation, preserving the contrast of both white and gray matter; convexity (of the cerebrum and cerebellum) is almost the same as that of T2-weighted image
3	Good contour continuation, preserving the contrast of both white and gray matter; convexity (of the cerebrum and cerebellum) is preserved but is less pronounced compared with that of T2-weighted image
2	Poor contour continuation; discontinuity can be seen in some parts; convexity is lost
1	Contour continuation is lost; concave contour is observed
0	Very concave (opposite of the natural convexity of cerebrum and cerebellum), with significant distortion

brain.[14] Such acquisition schemes are of particular interest for DWI and DTI in the CVJ area prone to strong susceptibility artifacts, and we have evaluated their potential in examining the CVJ.

Materials and Methods

DTI images were acquired from 10 healthy volunteers (7 men and 3 women; mean age 36.7 ± 9.6 years) using a 3T MR scanner (Magnetom Tim Trio System; Siemens, Erlangen, Germany) with a 32-channel head coil. The study was approved by an institutional review board and informed consent was obtained from all volunteers before scanning.

RS-EPI DTI images were acquired with 2D navigator-based reacquisition and parallel imaging[11] with the following parameters: matrix size = 166 × 166; FOV = 166 mm × 166 mm; section thickness = 3 mm; 20 sections; readout segments = 7; acceleration factor R = 2; TR = 5200 ms; TE = 83 ms; echo spacing = 0.38 ms; echo reading time = 208 μs; total signal intensity reading time = 31 ms; scan time: 9.44 minutes (1 repetition). SS-EPI DTI images were acquired for comparison with RS-EPI using the same parameters, except for acceleration factor: R = 3; TR = 5000 ms; TE = 90 ms; echo spacing = 1.1 ms; echo reading time = 848 μs; total signal intensity reading time = 59 ms; scan time: 9.37 minutes (8 repetitions). The number of repetitions was chosen to balance the acquisition time of both sequences, and avoid bias in intrinsic signal intensity–to-noise ratio estimation. Images were acquired in coronal orientation, with phase-encoding direction from right to left to make geometric distortion clearer for evaluation. For both approaches, full k-space acquisitions were used and the DTI protocol consisted of 1 acquisition at $b = 0$, and 12 diffusion encoding directions at $b = 1000$ seconds/mm². T2-weighted images were acquired in coronal orientation, and in the same location with diffusion tensor imaging for anatomic reference, with the following parameters: matrix size = 448 × 359; FOV = 220 mm × 178 mm; section thickness = 3.0 mm; 20 sections without gap; acceleration factor R = 2; TR = 3200 ms; TE = 79 ms; scan time: 1.44 minutes. Diffusion tensor calculation and image analyses were performed using DTIStudio software version 3.0.3 (Johns Hopkins University, Baltimore, Maryland). Maps of the trace of the diffusion tensor (which is equivalent to MD) and color-coded fiber orientation maps were evaluated by 2 independent neuroradiologists (with 4 and 15 years of experience, respectively), based on the anatomic information of T2-weighted images. The contours (of the cerebrum and the cerebellum) were evaluated on the diffusion trace images, and the delineation of fine structures was evaluated on the orientation maps. Four sets of features were evaluated:

1) Distortion using a semiquantitative scale of 0–4 (Table 1): Distortion was evaluated on the diffusion trace images at selected landmarks (contours of temporal base [lateral, inferior], parietal lobe, cerebellum [lateral, inferior], brain stem [center, margin], trigeminal nerve, and acoustic nerve).

2) Distortion (quantitative evaluation): For quantitative evaluation of distortion, image fusion between diffusion trace images and T2-weighted images was performed with AquariusNET Viewer (TeraRecon, San Mateo, California). For consistency, sections at the level of the red nucleus were chosen for the evaluation of geometric distortion at the temporal base, and sections where the dentate nucleus was the most clearly identified were used for the evaluation of cerebellar distortion. Distortion was measured as the maximum distance in the transverse (phase-encoding) direction between the brain borders on the trace image and the T2-weighted image (examples are shown in Fig 1*D*, -*G*). The distances measured on the left and right sides were added together.

3) Delineation of fine structures using a semiquantitative scale of 0–4 (Table 2): Delineation of fine structures was evaluated on the color-coded fiber orientation maps at selected landmarks (cerebellar vermis, temporal gyrus, decussation of internal arcuate fibers, cerebellar peduncle [superior, middle], cerebral fornix, laterality of basal ganglia, brain stem, and pyramidal tract).

4) SNR: The exact calculation of the SNR is not a trivial issue when multichannel coils, parallel imaging, and reconstruction filters are used.[15] In this case, the absolute SNR cannot be adequately evaluated using a background region, unless adequate corrections are made to take into account the noncentral χ^2 distribution of the noise.[16] As our point was just to compare SNR efficiency of RS-EPI and SS-EPI, we only estimated the SNR ratio between these 2 methods from the signal intensity and standard deviation taken directly in ROIs located in tissues (raw images acquired with $b = 0$ seconds/mm²). This approach is justified because, in such ROIs, the noise distribution remains Gaussian,[16] and the ROI locations and coil-array set up were exactly the same for RS-EPI and SS-EPI. ROIs were taken within the pons, corpus callosum, and thalamus.

Scores were analyzed with Wilcoxon signed rank tests, and distortion measurements were analyzed using a paired t test. A P value <0.05 was considered statistically significant. The interobserver variability between both radiologists was evaluated using interrater agreement (κ).

Results

There was an excellent correlation between both radiologists (weighted κ was 0.815 for RS-EPI and 0.883 for SS-EPI); hence, both scores were averaged.

Distortion Using a Semiquantitative Scale

The distortion of the temporal and cerebellar base in SS-EPI images was prominent compared with RS-EPI (Fig 1*B*, -*E*). The natural lateral contours of the temporal lobe on the T2-weighted image became prominently distorted on the SS-EPI image, while the convex shape was preserved on the RS-EPI image. The results of the mean distortion scales of RS-EPI and SS-EPI are shown in Table 3. Overall, RS-EPI ranked significantly higher compared with SS-EPI in 7/9 locations ($P < .01$). Notably, the scales of contours of the temporal lobe and the cerebellum on RS-EPI images were significantly higher than those on SS-EPI images ($P < .01$). The contour of the temporal lobe and the cerebellum were better delineated, and distortion artifacts were clearly reduced, with the RS-EPI compared
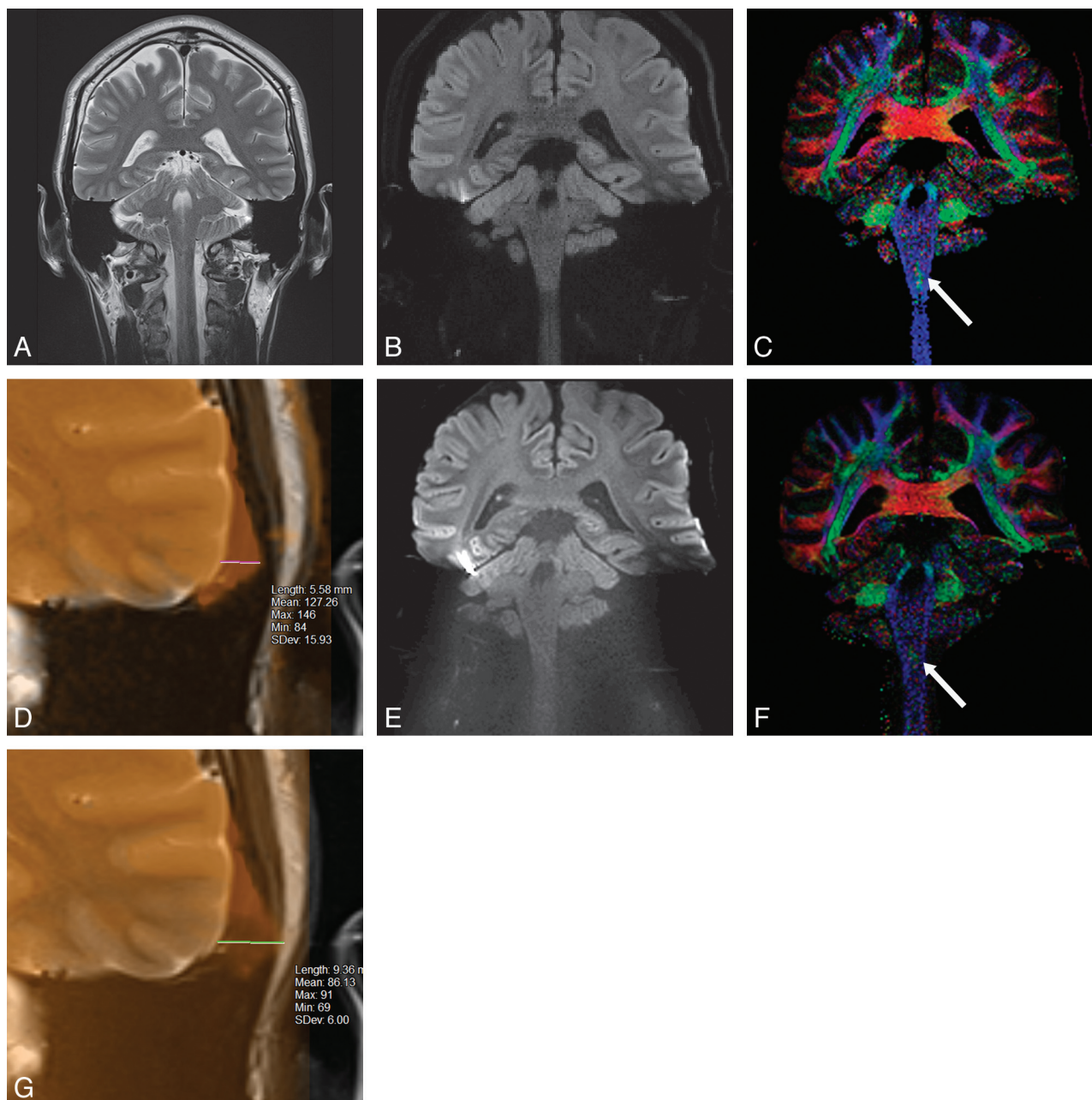
Fig 1. 40-year-old healthy male volunteer. Coronal MR images of brain obtained at the same level: *A*, T2-weighted image, (*B*) RS-EPI diffusion trace image, (*C*) RS-EPI color-coded fiber orientation map, (*D*) the fusion image of RS-EPI and T2-weighted image of left temporal lobe, (*E*) SS-EPI diffusion trace image, (*F*) SS-EPI color-coded fiber orientation map, (*G*) the fusion image of SS-EPI and T2-weighted image of left temporal lobe. The natural lateral contour of the left temporal lobe in the T2-weighted image (*A*) becomes prominently distorted in the SS-EPI image (*E*), but the convex shape manages to be preserved in the RS-EPI image (*B*). The decussation of the internal arcuate fibers is seen at the medulla level on the RS-EPI image (*C, arrow*), more clearly compared with the SS-EPI image (*F, arrow*). The distance between the contours of the left temporal base is 5.58 mm for RS-EPI (*D*), and 9.36 mm for SS-EPI (*G*).

with the SS-EPI. Fine structures were less distorted in the acoustic nerve and the trigeminal nerve with RS-EPI, but there was no significant difference in the brain stem (margin) or the parietal lobe.

Distortion (Quantitative Evaluation)

The absolute distances between the contours of the temporal base and the cerebellum visible on the diffusion trace images for RS-EPI and SS-EPI, and the corresponding T2-weighted images, are given in Fig 2. The mean distance at the temporal base is 6.46 mm for RS-EPI and 12.92 mm for SS-EPI. For the cerebellum, the

mean distance is 5.51 mm for RS-EPI and 8.95 mm for SS-EPI. Overall, the amount of distortion was significantly reduced with RS-EPI compared with SS-EPI ($P < .01$).

Delineation of Fine Structures

The results of the mean delineation scales of RS-EPI and SS-EPI are shown in Table 4. The temporal gyrus and the decussation of the internal arcuate fibers on the RS-EPI images were significantly better delineated compared with the SS-EPI images ($P < .01$). The delineation example of the decussation of the internal arcuate fibers is shown in Fig 1*C* and Fig 1*F*. The

Table 2: Delineation of fine structures using a semiquantitative scale	
	Scale (0–4)
4	Excellent; very good color contrast and discriminates with surrounding structure
3	Relatively good; very good color contrast and discriminates with surrounding structure
2	Enough good contrast with surrounding structure
1	Subtle, faint contrast with surrounding structure
0	Colors at border area are mixed; impossible to make diagnosis

Table 3: The result of mean scales of RS-EPI and SS-EPI (distortion)			
	RS-EPI	SS-EPI	P Value
Contours of temporal base			
Lateral	2.2 ± 0.5	0.4 ± 0.5	<0.01
Inferior	1.7 ± 0.6	0.0 ± 0.0	<0.01
Parietal lobe	3.9 ± 0.2	3.7 ± 0.3	0.14
Cerebellum			
Lateral	2.6 ± 0.8	0.4 ± 0.3	<0.01
Inferior	2.7 ± 0.7	0.6 ± 0.4	<0.01
Brain stem			
Center	3.4 ± 0.5	2.2 ± 0.9	<0.01
Margin	3.7 ± 0.3	3.0 ± 0.7	0.06
Trigeminal nerve	3.0 ± 0.7	1.8 ± 0.8	<0.01
Acoustic nerve	2.3 ± 0.6	1.1 ± 0.6	<0.01

cerebellar vermis and the laterality of the basal ganglia on RS-EPI were also significantly better delineated compared with SS-EPI ($P < .05$).

The cerebellar peduncle, the cerebral fornix, the brain stem, and the pyramidal tract were more clearly delineated with RS-EPI, but these differences were not as significant.

SNR

The SNR ratios between RS-EPI and SS-EPI at the 3 selected locations were 0.43 for the pons, 0.36 for the corpus callusom, and 0.41 for the thalamus. The average RS-EPI/SS-EPI SNR ratio was 0.40.

Discussion

DTI is a well-established method for neurologic applications. However, DTI has not yet been used extensively for the evaluation of CVJ lesions, because DTI images obtained with the standard SS-EPI DTI sequences are prone to severe susceptibility artifacts. CVJ lesions pose significant challenges to cranial, spine, and neurosurgeons because of the complex anatomy, and distortion-free images are essential for precisely evaluating CVJ structures and lesions, especially when microsurgery is planned.[17,18] Furthermore, fractional anisotropy has been shown to be a good clinical biomarker in detecting the lesions in the brain stem or the posterior fossa, as well as effects of radiation therapy.[19-21] Acute stroke lesions in the brain stem are also often missed by DWI because of susceptibility artifacts.[22,23]

Here we show that RS-EPI results—qualitatively and quantitatively—in significantly less distortion than SS-EPI in the diffusion trace images, especially at the base of the temporal lobe and the cerebellum. Overall RS-EPI was better than SS-EPI in 7/9 of our landmark locations. Delineation of fine structures on the orientation color maps was significantly better with RS-EPI in 4/9 locations, especially in the temporal gyrus

and the decussation of the internal arcuate fibers. Clearly, diffusion images (trace images and color maps) obtained with the RS-EPI sequence were much less artifacted than those obtained with the SS-EPI. Other groups have made efforts to decrease the amount of distortion of, or to obtain better delineation for, intracranial lesions with various DWI acquisition methods.[5,24-27] As far as we know, however, this is the first study to evaluate the level of geometric distortion in the CVJ obtained with RS-EPI and SS-EPI. The superiority of RS-EPI over SS-EPI has been shown in DWI of the pediatric brain.[14]

The main drawbacks of SS-EPI sequences are image distortion and blurring. SS-EPI requires long echo trains and long TEs to encode full k-space within only 1 echo signal intensity. T2/T2* decay during signal intensity acquisition leads to image blurring, while phase shift accumulation from local field inhomogeneities[28,29] results in geometric distortion. Image distortion can be decreased significantly by reducing the acquisition time of k-space points along the readout-encoding direction. With RS-EPI, this reduction is obtained by partitioning k-space into segments along the readout direction. This RS-EPI acquisition scheme was combined with the GRAPPA parallel acquisition to further reduce the signal intensity reading time in this study (the total signal intensity reading time was 31 ms for RS-EPI and 59 ms for SS-EPI). As a result, RS-EPI with GRAPPA yielded much faster k-space acquisition for each excitation and shorter TE compared with SS-EPI, significantly reducing the effect of susceptibility and T2* decay,[11,28] thus contributing to less distortion and blurring. This reduction in acquisition time for each segment, however, is accompanied by an enlargement of the acquisition bandwidth, which decreases SNR. Indeed, the SNR in our RS-EPI images
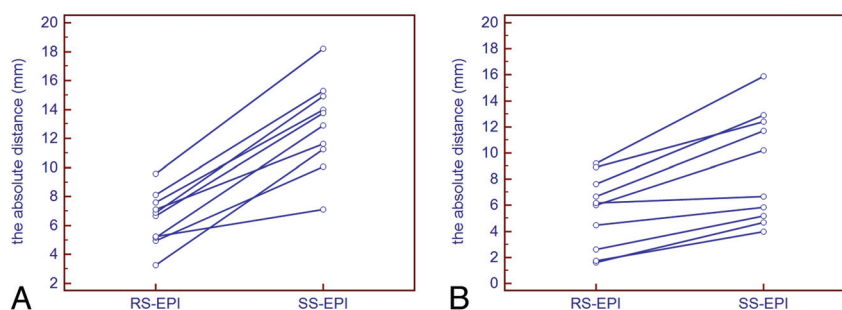

Fig 2. *A*, Distortion measurements at the level of the temporal base. *B*, Distortion measurements at the level of the cerebellum. The absolute distances between the contours of the temporal base (*A*) and the cerebellum (*B*), visible on the diffusion trace images for RS-EPI and SS-EPI and the corresponding T2-weighted images, are shown. The amount of distortion is significantly reduced with RS-EPI compared with SS-EPI ($P < .01$).

Table 4: The result of mean scales of RS-EPI and SS-EPI (delineation of fine structure)

	RS-EPI	SS-EPI	P Value
Cerebellar vermis	3.4 ± 0.5	2.2 ± 0.7	<0.05
Temporal gyrus	3.3 ± 0.4	1.2 ± 0.8	<0.01
Decussation of the internal arcuate fibers	3.3 ± 0.9	1.6 ± 0.8	<0.01
Cerebellar peduncle			
Superior	4.0 ± 0.0	3.9 ± 0.3	0.34
Middle	3.6 ± 0.3	2.8 ± 0.7	0.06
Cerebral fornix	4.0 ± 0.1	3.7 ± 0.6	0.24
Laterality of basal ganglia	3.6 ± 0.3	2.8 ± 0.6	<0.05
Brain stem	3.4 ± 0.6	2.5 ± 0.7	0.07
Pyramidal tract	3.7 ± 0.3	3.2 ± 0.5	0.06

was slightly less than half of that in SS-EPI images obtained with comparable acquisition times. Good SNR is essential for DTI to avoid bias in the estimated diffusion tensor parameters, especially in highly anisotropic white matter structures.

Another potential limitation of RS-EPI is that it requires longer overall acquisition times compared with SS-EPI, as each segment in *k*-space requires a separate acquisition, and it also corrects for effects of patient motion.[30] Indeed, an important feature of the current RS-EPI approach is that *k*-space segments that have been corrupted by motion, as detected from 2D navigator echoes, are reacquired,[11] which may increase the acquisition time (this can be used with SS-EPI[31]). Clearly, work is needed to reduce acquisition times.[32] No ghosting or motion artifacts could be detected in our images; however, we could not perform a quantitative evaluation of motion artifacts. To reach a high spatial resolution (1.0 mm × 1.0 mm), the FOV was kept as small as possible (166 mm × 166 mm), which resulted in the brain occupying most of the image and the surrounding background not being visible.

Conclusions

The amount of geometric distortion in diffusion images was much reduced with RS-EPI, and a better delineation of CVJ internal structure was possible compared with SS-EPI, despite using the same spatial resolution. Clearly, RS-EPI is much less sensitive to susceptibility artifacts, potentially offering clinical advantages in the detection of acute brain stem infarction, brain and skull base tumors, and inflammation, or the evaluation of the precise inner structure in the brain stem and cerebellum before surgery.

References

1. Le Bihan D. **Looking into the functional architecture of the brain with diffusion MRI.** *Nat Rev Neurosci* 2003;4:469–80
2. Sundgren P, Dong Q, Gomez-Hassan D, et al. **Diffusion tensor imaging of the brain: review of clinical applications.** *Neuroradiology* 2004;46:339–50
3. Forbes KP, Pipe JG, Karis JP, et al. **Improved image quality and detection of acute cerebral infarction with PROPELLER diffusion-weighted MR imaging.** *Radiology* 2002;225:551–55
4. Le Bihan D, Mangin JF, Poupon C, et al. **Diffusion tensor imaging: concepts and applications.** *J Magn Reson Imaging* 2001;13:534–46
5. Yamashita K, Yoshiura T, Hiwatashi A, et al. **Detection of middle ear cholesteatoma by diffusion-weighted MR imaging: multishot echo-planar imaging compared with single-shot echo-planar imaging.** *AJNR Am J Neuroradiol* 2011;32:1915–18
6. Robson MD, Anderson AW, Gore JC. **Diffusion-weighted multiple shot echo planar imaging of humans without navigation.** *Magn Reson Med* 1997;38:82–88
7. Griswold MA, Jakob PM, Heidemann RM, et al. **Generalized autocalibrating partially parallel acquisitions (GRAPPA).** *Magn Reson Med* 2002;47:1202–10
8. Bammer R, Stollberger R, Augustin M, et al. **Diffusion-weighted imaging with navigated interleaved echo-planar imaging and a conventional gradient system.** *Radiology* 1999;211:799–806
9. Butts K, de Crespigny A, Pauly JM, et al. **Diffusion-weighted interleaved echo-planar imaging with a pair of orthogonal navigator echoes.** *Magn Reson Med* 1996;35:763–70
10. Nunes RG, Jezzard P, Behrens TEJ, et al. **Self-navigated multishot echo-planar pulse sequence for high-resolution diffusion-weighted imaging.** *Magn Reson Med* 2005;53:1474–78
11. Porter DA, Heidemann RM. **High resolution diffusion-weighted imaging using readout-segmented echo-planar imaging, parallel imaging and a two-dimensional navigator-based reacquisition.** *Magn Reson Med* 2009;62:468–75
12. Heidemann RM, Porter DA, Anwander A, et al. **Diffusion imaging in humans at 7T using readout-segmented EPI and GRAPPA.** *Magn Reson Med* 2010;64:9–14
13. Holdsworth SJ, Skare S, Newbould RD, et al. **Readout-segmented EPI for rapid high resolution diffusion imaging at 3T.** *Eur J Radiol* 2008;65:36–46
14. Holdsworth S, Yeom K, Skare S, et al. **Clinical application of readout-segmented–echo-planar imaging for diffusion-weighted imaging in pediatric brain.** *AJNR Am J Neuroradiol* 2011;32:1274–79
15. Dietrich O, Raya JG, Reeder SB, et al. **Measurement of signal-to-noise ratios in MR images: Influence of multichannel coils, parallel imaging, and reconstruction filters.** *J Magn Reson Imaging* 2007;26:375–85
16. Brion V, Poupon C, Riff O, et al. **Parallel MRI noise correction: an extension of the LMMSE to noncentral χ distributions.** *Med Image Comput Comput Assist Interv* 2011;14:226–33
17. Karam YR, Menezes AH, Traynelis VC. **Posterolateral approaches to the craniovertebral junction.** *Neurosurgery* 2010;66:A135–40
18. Visocchi M, Della Pepa GM, Doglietto F, et al. **Video-assisted microsurgical transoral approach to the craniovertebral junction: personal experience in childhood.** *Childs Nerv Syst* 2011;27:825–31
19. Lui YW, Law M, Chacko-Mathew J, et al. **Brainstem corticospinal tract diffusion tensor imaging in patients with primary posterior fossa neoplasms stratified by tumor type: a study of association with motor weakness and outcome.** *Neurosurgery* 2007;61:1199–207
20. Helton KJ, Weeks JK, Phillips NS, et al. **Diffusion tensor imaging of brainstem tumors: axonal degeneration of motor and sensory tracts.** *J Neurosurg Pediatr* 2008;1:270–76
21. Rueckriegel SM, Driever PH, Blankenburg F, et al. **Differences in supratentorial damage of white matter in pediatric survivors of posterior fossa tumors with and without adjuvant treatment as detected by magnetic resonance diffusion tensor imaging.** *Int J Radiat Oncol Biol Phys* 2010;76:859–66
22. Küker W, Weise J, Krapf H, et al. **MRI characteristics of acute and subacute brainstem and thalamic infarctions: value of T2-and diffusion-weighted sequences.** *J Neurol* 2002;249:33–42
23. Chalela JA, Kidwell CS, Nentwich LM, et al. **Magnetic resonance imaging and computed tomography in emergency assessment of patients with suspected acute stroke: a prospective comparison.** *Lancet* 2007;369:293–98
24. Koch M, Glauche V, Finsterbusch J, et al. **Distortion-free diffusion tensor imaging of cranial nerves and of inferior temporal and orbitofrontal white matter.** *Neuroimage* 2002;17:497–506
25. Hori M, Ishigame K, Shiraga N, et al. **Mean diffusivity, fractional anisotropy maps, and three-dimensional white-matter tractography by diffusion tensor imaging. Comparison between single-shot fast spin-echo and single-shot echo-planar sequences at 1.5 Tesla.** *Eur Radiol* 2008;18:830–34
26. Nagae-Poetscher LM, Jiang H, Wakana S, et al. **High-resolution diffusion tensor imaging of the brain stem at 3 T.** *AJNR Am J Neuroradiol* 2004;25:1325–30
27. Brockstedt S, Moore JR, Thomsen C, et al. **High-resolution diffusion imaging using phase-corrected segmented echo-planar imaging.** *Magn Reson Imaging* 2000;18:649–57
28. Holdsworth SJ, Skare S, Newbould RD, et al. **Robust GRAPPA-accelerated diffusion-weighted readout-segmented (RS)-EPI.** *Magn Reson Med* 2009;62:1629–40
29. Skare S, Newbould RD, Clayton DB, et al. **Clinical multishot DW-EPI through parallel imaging with considerations of susceptibility, motion, and noise.** *Magn Reson Med* 2007;57:881–90
30. Mukherjee P, Chung S, Berman J, et al. **Diffusion tensor MR imaging and fiber tractography: technical considerations.** *AJNR Am J Neuroradiol* 2008;29:843–52
31. Benner T, van der Kouwe AJW, Sorensen AG. **Diffusion imaging with prospective motion correction and reacquisition.** *Magn Reson Med* 2011;66:154–67
32. Naganawa S, Kawai, H., et al. **Anatomical details in brainstem and cisterns by RESOLVE with undirectional MPG; comparison with single-shot EPI diffusion weighted image.** *Proceedings of the 19th International Society for Magnetic Resonance in Medicine*, Montreal, Canada, 2011:4248